Low-Thrust to Solar-Sail Trajectories:

A Homotopic Approach

Nicola Sullo[1], Alessandro Peloni[2], and Matteo Ceriotti[3]

University of Glasgow, Glasgow G12 8QQ, United Kingdom

This paper describes a novel method to compute minimum-time solar-sail trajectories starting from a given low-thrust solution. The method is based on the use homotopy and numerical continuation. Homotopy is used to link the low-thrust with the solar-sail optimal control problem. Numerical continuation is used to compute the optimal solar-sail solution, starting from a given low-thrust planar solution, which is normally easy to find. Planar solar sail trajectories are computed by means of the homotopic approach. These solutions are used to compute, in a single shooting approach, three-dimensional solar-sail trajectories, for transfer scenarios involving a small change of the orbital inclination. The proposed homotopic approach is tested against a conventional approach, based on the use of a genetic algorithm. Numerical test cases are performed both on Earth-Mars and Earth-Apophis rendezvous. The results show that the proposed method is advantageous, in terms of accuracy of the solution and computational time.

Nomenclature

a	= semi-major axis, AU
$\bar{a}$	= real positive scaling factor

[1] Ph.D. Candidate, School of Engineering, James Watt (South) Building; n.sullo.1@research.gla.ac.uk. Student member AIAA.

[2] Ph.D. Candidate, School of Engineering, James Watt (South) Building; a.peloni.1@research.gla.ac.uk. Student member AIAA.

[3] Lecturer, School of Engineering, James Watt (South) Building; matteo.ceriotti@glasgow.ac.uk. Member AIAA.

a_c = solar-sail characteristic acceleration, $\mathrm{mm/s^2}$

$a_{\max}$ = maximum low-thrust acceleration, $\mathrm{mm/s^2}$

$\boldsymbol{a}$ = acceleration vector

A, B, C, D = multiplication factors of the Hamiltonian expansion

e = eccentricity

$\boldsymbol{f}_a$ = propulsive acceleration, $\mathrm{mm/s^2}$

H = Hamiltonian

$\tilde{H}$ = reduced Hamiltonian

i = inclination, deg

J = cost function, days

m = number of nonlinear equations of the shooting function

n = number of optimization variables

$\hat{\boldsymbol{n}}$ = thrust-induced acceleration unit vector

r = radial position, AU

$\hat{\boldsymbol{r}}$ = radial unit vector

$r_{\oplus}$ = mean Sun-Earth distance, 1 AU

t = time, days

t_{0f} = time of flight, days

u = velocity along $\hat{\boldsymbol{r}}$, km/s

$\bar{u}$ = low-thrust non-dimensional control

v = velocity along $\hat{\boldsymbol{\vartheta}}$, km/s

w = velocity along $\hat{\boldsymbol{\varphi}}$, km/s

$\boldsymbol{x}$ = state vector

$\bar{\boldsymbol{x}}_0$ = initial state of the departing object

$\bar{\boldsymbol{x}}_f$ = final state of the target object

$\hat{\boldsymbol{X}}, \hat{\boldsymbol{Y}}, \hat{\boldsymbol{Z}}$ = set of basis vectors of the heliocentric ecliptic frame

$\boldsymbol{z}$ = vector of the optimization variables

α = cone angle, deg

β = clock angle, deg

γ = solar-sail lightness number

ε = homotopic-transformation parameter

ϑ = longitude, deg

$\hat{\boldsymbol{\vartheta}}$ = longitude unit vector

$\boldsymbol{\lambda}$ = costate vector, $\left(\lambda_r, \lambda_\vartheta, \lambda_\varphi, \lambda_u, \lambda_v, \lambda_w\right)$

μ = Sun's gravitational parameter, $1.3271\times10^{11}\ \mathrm{km}^3/\mathrm{s}^2$

ν = true anomaly, deg

τ = parameter dependent on the cone angle

φ = latitude, deg

$\hat{\boldsymbol{\varphi}}$ = latitude unit vector

$\boldsymbol{\Phi}$ = shooting function

$\boldsymbol{\psi}$ = vector of boundary conditions

ω = argument of pericenter, deg

Ω = right ascension of the ascending node, deg

Superscripts

T = transpose

$\cdot$ = time derivative

$*$ = ideal value

Subscripts

0	= initial desired value
1	= first continuation
2	= second continuation
$2D$	= two-dimensional case
$3D$	= three-dimensional case
f	= final desired value
LT	= low thrust
SS	= solar sail
$LTSS$	= low-thrust to solar-sail homotopic transformation

I. Introduction

Low-thrust propulsion, such as the one produced by an electric thruster, is currently one of the most promising propulsion systems for interplanetary missions. On the other hand, solar sailing is an appealing technology, for being propellant-less. In general, for the design of both low-thrust and solar-sail trajectories, since no analytical solutions exist, an optimal control problem (OCP) must be solved numerically [1, 2].

A common approach used to compute solar-sail optimal transfers consists in the use of the indirect method, which is based on the Pontryagin Minimum Principle (PMP) formulation [3]. One of the first applications of the PMP formulation to interplanetary solar-sail transfers is by Sauer [4]. More recent studies focused on the use of the indirect method in computing optimal transfer trajectories for a non-ideal solar sail [5, 6] and for optimal solar-sail transfers to near-Earth asteroids [7, 8]. Pseudo-spectral methods with direct transcription are an alternative [9]: this method, combined with a shape-based approach to generate a first guess, has also been used to design optimal solar-sail trajectories for multiple near-Earth-asteroid rendezvous missions [10]. Single- or multiple-shooting differential-correction processes are also employed to generate solar-sail trajectories [11, 12]. The trajectories obtained are often used as initial-guess solutions for a subsequent optimisation, usually via direct transcription and pseudo-spectral methods. Furthermore, a heuristic evolutionary method has also been employed to design optimal very-low-thrust transfers powered by solar-sail propulsion [13]. Heuristic methods are also used in literature as automatized techniques to solve space-transfer OCPs via the PMP formulation (also referred to as Hamiltonian formulation) [14-16]. In addition, in

[16] optimal low-thrust, solar-sail, and hybrid low-thrust/solar-sail trajectories are computed for the cases of planar circular-to-circular orbit transfer problems. According to that paper, the optimal control problems considered have all been individually computed (within the Hamiltonian formulation) by means of the combined use of a genetic algorithm and a gradient-based method.

One of the main advantages of the indirect optimization method consists in the highly accurate solutions produced if it converges. However, it often suffers (for a wide range of problems) of numerical sensitivity to the initial-guess solution provided, so that a convergent solution can be hard to obtain [17]. To address this difficulty, techniques based on the combined use of homotopy and continuation have been extensively applied in literature. The homotopy [18] is used to relax the OCP to one for which a solution is already known or easy to compute. Numerical continuation [19, 20] is employed in order to evolve the solution of the relaxed OCP to the one of the original optimal control problem. For the sake of simplicity in the explanation, in this paper, the homotopy and continuation techniques are often enclosed under the general family of homotopy methods.

Conspicuous work has been carried out regarding the application of these techniques, especially (but not only) related to the computation of optimal low-thrust transfers. Several studies have involved homotopic approaches for the solution of fuel-optimal low-thrust transfers. In 2002, Bertrand and Epenoy [21] studied the use of homotopy in order to relax a bang-bang optimal control problem to one characterized by a smoother control. Then, they used continuation in order to transform the relaxed problem to the original one. Finally, they also provided an example of the application of their method to the computation of a low-thrust fuel-optimal interplanetary transfer. Later in 2004, Haberkorn et al. [22] solved the low-thrust minimum-fuel orbital transfer problem by using two homotopies in series: a first one on the initial conditions of the optimal control problem (to solve the energy-optimal transfer), a second one on the problem cost function, thus connecting the energy to the fuel OCP. In 2012, the energy-to-fuel homotopic criterion was resumed by Li and Xi [23] and applied to solve a different kind of trajectory optimization problem, that is a low-thrust minimum-fuel formation-flying satellites reconfiguration. A different homotopic approach has also been developed to compute minimum-time low-thrust trajectories. In 2003, Caillau et al. [24] solved a low-thrust minimum-time-of-flight orbital transfer problem by applying the homotopy method on the maximum thrust provided by the propulsion system. Homotopy methods have been successfully employed even in the computation of optimal low-thrust transfers in the planar restricted three-body Earth-Moon system. In fact, in 2012, Picot [25] computed

minimum-time-of-flight and minimum-energy Earth-L_2 and Earth-Moon low-thrust trajectories by means of the homotopy method. The minimum-time transfers were obtained by continuation on the control bound, the minimum-energy transfers, instead, via continuation on the parameter relative to the mass ratio of the primaries. A combined use of homotopy with other optimization methods has been also introduced, to address the problem of initialization of the homotopic-continuation process. For instance, Guo et al. [26] proposed the use of a pseudo-spectral method to solve the energy-optimal problem and provide a good initial-guess solution for the subsequent energy-fuel homotopic continuation. Jiang et al. [27], instead, proposed the use of a particle-swarm optimization algorithm to increase the probabilities to find a global solution for the minimum-energy problem. Starting from such solution, they used the energy-fuel homotopy in order to compute minimum-fuel low-thrust rendezvous with the inclusion of gravity assist maneuvers. Studies have been also carried out in which the homotopy method has been employed for the computation of high-fidelity optimal low-thrust transfers, inclusive of several external constraints. In this regard, Geffroy and Epenoy [28] used numerical averaging techniques to introduce various constraints in the OCP formulation for low-thrust transfer trajectories. These constraints are both environmental (Earth oblateness and shadow effects) and technological (maximum thrust-magnitude and direction constraints). Then, the authors computed both minimum-time and minimum-fuel optimal solutions; the latter were obtained by employing the energy-fuel homotopy and using the minimum-time-of-flight solution as initial-guess to initialize the continuation. Furthermore, in [28] the authors proposed also a continuation strategy to consider the thrust-direction constraint, by progressively reducing the boundaries on the thrust cone-angle until the required value. In 2013, Tarzi et al. [29] resumed the work in [28] and improved it by considering additional environmental constraints in the OCP formulation and enhancing the convergence and speed of the optimization process. Very recently in 2016, Pan et al. [30] proposed a double-homotopy method to overcome some of the main difficulties that not infrequently lead traditional homotopy method to fail during the continuation process. The authors showed the effectiveness of the method also on a trajectory optimization problem, relative to a three-dimensional (3D) minimum-time low-thrust orbital transfer.

Despite an extensive application of the homotopy method to trajectory optimization problems with low-thrust propulsion, a proper literature is missing about its use for the solution of optimal transfer problems with solar-sail propulsion. Although solar-sail propulsion represents a particular form of low-thrust propulsion, a solar sail differs

from an electric propulsion because: (a) a solar sail cannot thrust towards the Sun, and (b) the magnitude of its acceleration is nonlinearly related to the thrust direction and it depends on the inverse of the square distance from the Sun. On the other hand, low-thrust propulsion, at least in a preliminary design phase, does not usually have such restrictions on the thrust provided [31]. Thus, due to its constraints, the solar-sail OCP is characterized by a more restricted space of feasible solutions with respect to the classical low-thrust one. That is, the solar-sail OCP is usually more difficult to solve numerically respect to a classical low-thrust one. Therefore, the use of the homotopy method could be an advantageous approach if employed to transform a low-thrust optimal solution into a solar-sail one. The solution of the low-thrust optimal control problem can be obtained by one of the conventional approaches available in the literature or by a preliminary application of the homotopy method.

The work in this paper focuses on the application of homotopy to convert low-thrust to solar-sail optimal trajectories. Furthermore, in this paper, the homotopy is applied for the first time (to the best of the author's knowledge) to change the thrust provided by a propulsion system into the one given by a different propulsion system. In particular, the purpose is to develop an efficient method to compute a solution for the solar-sail minimum-time-of-flight OCP, starting from a low-thrust solution of a similar transfer, which is easier to find or readily available. The efficiency of the proposed method regards both the computational time needed to get the solution and the level of accuracy of the solution itself. The method makes use of the homotopy theory associated with numerical continuation: the purpose is to properly link the low-thrust to the solar-sail minimum time-of-flight problem by means of a homotopy function. Consequently, it is possible to pass from the solution of the former OCP to the one of the latter OCP via the continuation method. Furthermore, numerical comparisons will address the problem to relate the method proposed to conventional approaches to numerically solve solar-sail optimal problems within the Hamiltonian formulation (as done, for instance, in [16]). The homotopic approach proposed in this paper is developed in the approximation of planar transfers. That is, only planar solar sail trajectories can be computed by this method. However, the planar solutions are proven to be good approximations of the 3D solar-sail solutions, for small-inclination-change transfers. This occurs in the numerical cases tested in this paper, in which the planar solar sail transfers are directly used to compute, in a single shooting approach, the 3D transfer solutions.

The paper is organized as follows. In Sec. II, the mathematical model is shown, whereas in Sec. III the homotopic approach is explained in detail. In Sec. IV, two numerical test cases on Earth-Mars rendezvous are used to validate

the approach proposed and compare it with a conventional heuristic-based method used to compute solar-sail optimal solutions. In the same section, the homotopic approach is also tested for the computation of transfers to an object with larger orbital eccentricity. That is done in two additional test cases, regarding Earth-Apophis rendezvous. Conclusions and final remarks are drawn in Sec. V.

II. Mathematical model

The core of the proposed approach consists of a homotopy function that links the low-thrust with the solar-sail optimal problem. Numerical continuation is used to compute the minimum-time solar-sail solution, starting from the low-thrust solution for a similar transfer problem. The low-thrust solution is assumed to be provided, as it can be computed without any particular effort. Specifically, the homotopic transformation is introduced on the acceleration that is provided by the low-thrust system, given by the expression

$$\boldsymbol{a}_{LT} = a_{\max}\bar{u}\,\hat{\boldsymbol{n}} \tag{1}$$

in which $a_{\max}$ and $\bar{u} \in [0,1]$ are, respectively, the low-thrust maximum acceleration and the non-dimensional control; $\hat{\boldsymbol{n}}$ is the thrust unit vector. Note that the spacecraft mass variation is not considered in the equations of the dynamics. This is because the optimal control law for a low-thrust-propelled spacecraft is transformed to that of a propellant-less sailcraft. The solar sail is modeled as an ideal and perfectly-reflecting sail, for which the acceleration provided is given by the expression

$$\boldsymbol{a}_{SS} = a_c \left(\frac{r_\oplus}{r}\right)^2 \left(\hat{\boldsymbol{r}}\cdot\hat{\boldsymbol{n}}\right)^2 \hat{\boldsymbol{n}} \tag{2}$$

in which a_c is the solar-sail characteristic acceleration, $r_\oplus$ is the mean Earth distance from the Sun, and r is the radial distance of the spacecraft from the Sun. The unit vector $\hat{\boldsymbol{r}}$ identifies the radial direction: $\boldsymbol{r} = r\,\hat{\boldsymbol{r}}$, as shown in Fig 1a.

A. Reference frames

Spherical coordinates have been used in the formulation of the equations of motion. These coordinates are based on the heliocentric ecliptic frame, which is identified by the set of basis vectors $\left\{\hat{\boldsymbol{X}},\hat{\boldsymbol{Y}},\hat{\boldsymbol{Z}}\right\}$ in Fig 1a. The state vector $\boldsymbol{x}$, in terms of spherical coordinates, is given by

$$\boldsymbol{x}=\begin{bmatrix} r & \vartheta & \varphi & u & v & w \end{bmatrix}^T \tag{3}$$

As in Fig 1a, ϑ and φ identify, respectively, the longitude and the latitude angles, u,v,w denote the components of the velocity vector along the directions of the orthonormal triad $\left\{\hat{\boldsymbol{r}},\hat{\boldsymbol{\vartheta}},\hat{\boldsymbol{\varphi}}\right\}$. The direction $\hat{\boldsymbol{n}}$ of the thrust is determined by the cone angle α and clock angle β, as shown in Fig 1b.

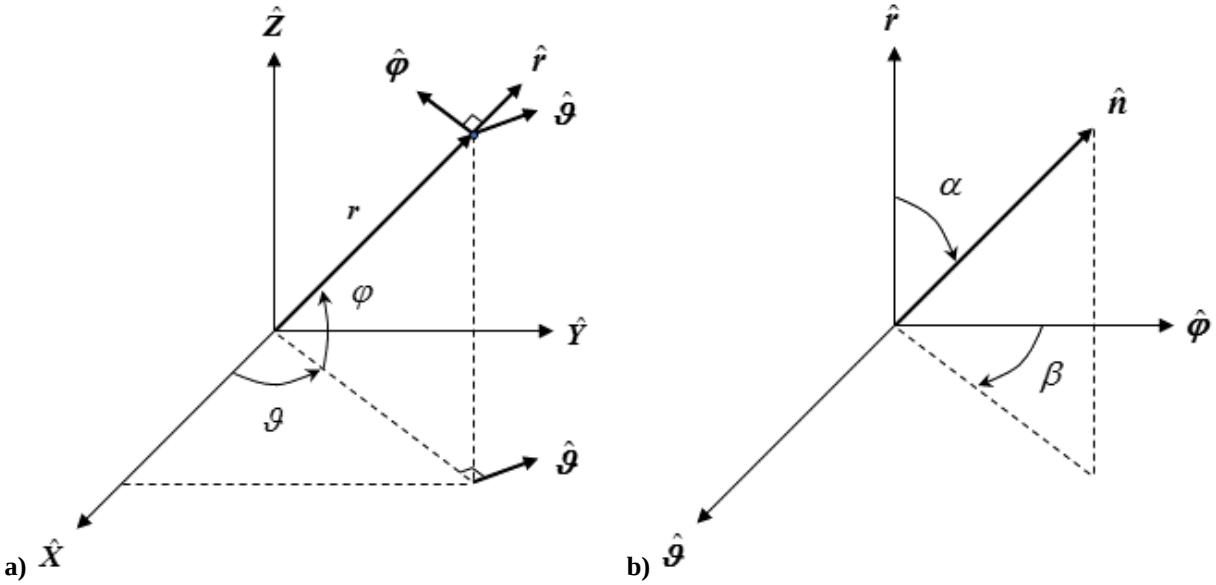

Fig 1. Reference frame and control angles. In (a) the heliocentric ecliptic frame. In (b) the cone and clock angles representation.

B. Equations of the dynamics

The dynamics of a spacecraft under the action of gravity and a generic acceleration are [32]

$$\dot{\boldsymbol{x}} = \begin{bmatrix} u \\ \dfrac{v}{r\cos\varphi} \\ \dfrac{w}{r} \\ \dfrac{v^2+w^2}{r} - \dfrac{\mu}{r^2} + \boldsymbol{f}_a \cdot \hat{\boldsymbol{r}} \\ \dfrac{vw\tan\varphi - uv}{r} + \boldsymbol{f}_a \cdot \hat{\boldsymbol{\vartheta}} \\ -\dfrac{v^2\tan\varphi + uw}{r} + \boldsymbol{f}_a \cdot \hat{\boldsymbol{\varphi}} \end{bmatrix} \tag{4}$$

in which $\boldsymbol{f}_a$ is the propulsive acceleration and μ refers to the Sun's gravitational parameter. For a low-thrust propelled spacecraft, the expression of $\boldsymbol{f}_a$, in terms of cone and clock angles, is given by

$$\boldsymbol{f}_a = a_{max}\bar{u}\begin{bmatrix} \cos\alpha \\ \sin\alpha\sin\beta \\ \sin\alpha\cos\beta \end{bmatrix},\ \alpha \in [0,\pi],\ \beta \in [0,2\pi] \tag{5}$$

whereas, for the case of a sailcraft, it is given by

$$\boldsymbol{f}_a = a_c\left(\frac{r_\oplus}{r}\right)^2 \cos^2\alpha \begin{bmatrix} \cos\alpha \\ \sin\alpha\sin\beta \\ \sin\alpha\cos\beta \end{bmatrix},\ \alpha \in \left[0,\frac{\pi}{2}\right],\ \beta \in [0,2\pi] \tag{6}$$

C. Optimal control problem formulation

The optimal control problem is stated for the general case of a minimum-time rendezvous, whereas the optimal control laws are initially formulated in the planar case, both for the low-thrust and the solar-sail transfers [2]. This is done because the planar low-thrust and solar-sail OCPs occur, respectively, at the beginning and the end of the homotopy continuation. Furthermore, the planar solar-sail solution is used to compute the 3D solar-sail trajectory, using a single shooting approach. The OCP formulation of the 3D solar-sail transfer is also given at the end of this section.

The equations of the dynamics of Sec. II.B are reduced to the planar case by considering $\varphi = w = 0$, $\beta = \dfrac{\pi}{2}$ and $\alpha \in [-\pi,\pi]$ for low-thrust propulsion or $\alpha \in \left[-\dfrac{\pi}{2},\dfrac{\pi}{2}\right]$ for solar-sail propulsion.

The cost function J to be minimized is the total transfer time, that is

$$J = t_{0f} = t_f - t_0 \tag{7}$$

in which t_0 and t_f are the initial and final epochs, respectively. It should be noted that the normal case [33] has been considered in the formulation of the optimal control problem. The first-order PMP conditions are considered and stated below. These conditions require the definition of the Hamiltonian function [2] as

$$H = \boldsymbol{\lambda} \cdot \dot{\boldsymbol{x}} \tag{8}$$

in which $\boldsymbol{\lambda} = \begin{bmatrix} \lambda_r & \lambda_\vartheta & \lambda_\varphi & \lambda_u & \lambda_v & \lambda_w \end{bmatrix}^T$ is the vector of the costates. Note that, for the case of planar transfers, $\lambda_\varphi = \lambda_w = 0$. The costate equations are given by

$$\dot{\boldsymbol{\lambda}} = -\frac{\partial H}{\partial \boldsymbol{x}} \tag{9}$$

The initial and final boundary conditions for a rendezvous problem are, respectively:

$$\boldsymbol{\psi}_0 = \boldsymbol{x}(t_0) - \bar{\boldsymbol{x}}_0 = \boldsymbol{0} \tag{10}$$

$$\boldsymbol{\psi}_f = \begin{bmatrix} \boldsymbol{x}(t_f) - \bar{\boldsymbol{x}}_f \\ H(t_f) + 1 - \boldsymbol{\lambda}(t_f) \cdot \dfrac{\partial \bar{\boldsymbol{x}}_f}{\partial t_f} \end{bmatrix} = \boldsymbol{0} \tag{11}$$

In Eq. (10), $\bar{\boldsymbol{x}}_0$ is the initial state of the departing object, whereas in Eq. (11), $\bar{\boldsymbol{x}}_f$ is the final state of the target object. The scalar condition in Eq. (11) is known as transversality condition on the Hamiltonian. The optimal control is derived by the minimization of the Hamiltonian function with respect to the control variables. The optimal control laws are stated both for the planar and the 3D case, with the hypothesis that no singular arcs occur. That is, $(\lambda_u, \lambda_v) \neq 0$ for the planar case and $(\lambda_u, \lambda_v, \lambda_w) \neq 0$ for the 3D case, for all $t \in [t_0, t_f]$. It is important to note that this hypothesis is numerically verified *a posteriori* in all the test cases shown in this paper.

Planar case. For the case of a low-thrust system, the optimal direction of the thrust is given by

$$\cos\alpha = -\frac{\lambda_u}{\sqrt{\lambda_u^2 + \lambda_v^2}}, \quad \sin\alpha = -\frac{\lambda_v}{\sqrt{\lambda_u^2 + \lambda_v^2}} \tag{12}$$

considering $\alpha \in [-\pi, \pi]$ and $\bar{u} = 1$ for all $t \in [t_0, t_f]$. The optimal control laws for α and $\bar{u}$ involve a continuous profile for the acceleration provided by the low-thrust system. For a sailcraft, the optimal direction of the thrust is given by

$$\tan\alpha = \left(\frac{-3\lambda_u - \sqrt{9\lambda_u^2 + 8\lambda_v^2}}{4\lambda_v} \right) \tag{13}$$

considering $\alpha \in \left[-\frac{\pi}{2}, \frac{\pi}{2} \right]$. It should be noted that Eq. (13) provides a continuous control law for the cone angle. That is, $\lim_{\lambda_v \to 0} \alpha = 0$ if $\lambda_u < 0$ and $\lim_{\lambda_v \to 0} \alpha = -\frac{\pi}{2}$ if $\lambda_u > 0$.

3D case. For the case of a 3D solar-sail transfer, the thrust direction is identified by both the cone and clock angles. Recalling the primer vector theory [3], the ideal thrust direction $\hat{\boldsymbol{n}}^*$ that minimizes the Hamiltonian is

$$\hat{\boldsymbol{n}}^* = -\frac{1}{\sqrt{\lambda_u^2 + \lambda_v^2 + \lambda_w^2}} \begin{bmatrix} \lambda_u \\ \lambda_v \\ \lambda_w \end{bmatrix} = \begin{bmatrix} \cos\alpha^* \\ \sin\alpha^* \sin\beta^* \\ \sin\alpha^* \cos\beta^* \end{bmatrix} \tag{14}$$

in which α^*, β^* are, respectively, the values of the cone and clock angle that identify the direction of $\hat{\boldsymbol{n}}^*$. Although thrusting along $\hat{\boldsymbol{n}}^*$ is feasible by a low-thrust system (resulting in the thrust direction given by Eq. (12), for the planar case), this is not always possible for the case of a sailcraft. In fact, a solar sail cannot thrust along $\hat{\boldsymbol{n}}^*$, if $\alpha^* \geq \frac{\pi}{2}$. However, it is possible to thrust in a direction (α, β) so that the thrust along $\hat{\boldsymbol{n}}^*$ is maximized. According to McInnes [34], the optimal cone and clock angles are given, in terms of α^* and β^*, by

$$\tan\alpha = \frac{-3 - \sqrt{9 + 8\tan^2\alpha^*}}{4\tan\alpha^*} \tag{15}$$

$$\beta = \beta^* \tag{16}$$

By combining Eq. (14) with Eq. (15) and Eq. (16), the optimal control laws for the cone and clock angles are given by

$$\tan\alpha = \frac{3\lambda_u + \sqrt{9\lambda_u^2 + 8\left(\lambda_v^2 + \lambda_w^2\right)}}{4\sqrt{\lambda_v^2 + \lambda_w^2}} \tag{17}$$

$$\cos\beta = -\frac{\lambda_w}{\sqrt{\lambda_v^2 + \lambda_w^2}}, \ \sin\beta = -\frac{\lambda_v}{\sqrt{\lambda_v^2 + \lambda_w^2}} \tag{18}$$

Note that, from Eq. (17), $\tan\alpha \geq 0$ and, therefore, the cone angle is always limited in $\alpha \in \left[0, \frac{\pi}{2}\right]$. In addition, it can be easily shown that $\lim_{\lambda_v^2 + \lambda_w^2 \to 0} \alpha = 0$ if $\lambda_u < 0$ and $\lim_{\lambda_v^2 + \lambda_w^2 \to 0} \alpha = \frac{\pi}{2}$ if $\lambda_u > 0$. This results in a continuous profile of the cone angle over its domain of existence. In addition, the clock angle resulting from Eq. (18) is continuous on $\beta \in [0, 2\pi]$, if considering $\left(\lambda_v, \lambda_w\right) \neq 0$. In the case $\left(\lambda_v, \lambda_w\right) = 0$, the value of β is undetermined. However, this occurrence is not considered because it would be either $\alpha = 0$ or $\alpha = \frac{\pi}{2}$: if $\alpha = 0$, the thrust direction is uniquely determined regardless of the clock angle; if $\alpha = \frac{\pi}{2}$, the solar sail does not provide any thrust and, therefore, the value of the clock angle is irrelevant. It is worth noting that the cone angle law for the 3D case turns into Eq. (13), if $\lambda_w = 0$ and $\beta^* = \frac{\pi}{2}$ are considered in Eq. (14).

III. Homotopic approach

The homotopy is defined as a function linking continuously two continuous functions from a topological space to another [18]. It is proposed to use the homotopy to link the shooting functions relative to the low-thrust and solar-sail OCPs, respectively. The shooting function is represented by a nonlinear function given by $\boldsymbol{\Phi}(\boldsymbol{z}) : \mathbb{R}^n \to \mathbb{R}^m$, in which n is the number of optimization variables and m is the number of nonlinear scalar equations included in $\boldsymbol{\Phi}$ [22, 27]. For the OCPs at hand, such function is expressed as

$$\boldsymbol{\Phi}(\boldsymbol{z}) = \boldsymbol{\psi}_f \tag{19}$$

in which $\boldsymbol{z}$ is the vector of the optimization variables given by the initial values of the costates $\boldsymbol{\lambda}(t_0)$ and the time of flight t_{0f}, as follows.

$$\boldsymbol{z} = \begin{bmatrix} \boldsymbol{\lambda}(t_0) & t_{0f} \end{bmatrix}^T \tag{20}$$

The zeros of the shooting function represent the solution of the optimal control problem. Therefore, the homotopy is represented by $\boldsymbol{\Phi}(\boldsymbol{z}, \varepsilon) : \mathbb{R}^n \times \mathbb{R} \to \mathbb{R}^m$, in which $\varepsilon \in [0,1]$ is the so-called homotopic-transformation parameter. When $\varepsilon = 0$, the homotopy is the shooting function relative to the low-thrust optimal problem, whereas, when $\varepsilon = 1$, the homotopy turns in the shooting function relative to the solar-sail optimal problem.

A. Homotopic transformation

As stated, a homotopic transformation is introduced to link the low-thrust with the solar-sail OCP. This transformation is related to the formulation of the spacecraft acceleration, and it is given by

$$\boldsymbol{f}_a = \boldsymbol{f}_{a,LTSS} = a_{\max} \left[(1-\varepsilon_1)\bar{u} + \left(\left(\frac{r_\oplus}{r} \right)^2 \cos^2 \alpha \right) \varepsilon_1 \right] \begin{bmatrix} \cos\alpha \\ \sin\alpha \end{bmatrix} \tag{21}$$

in which $\alpha \in [-\pi, \pi]$ and $\varepsilon \equiv \varepsilon_1$. The corresponding homotopy is

$$\boldsymbol{\Phi}_1(\boldsymbol{z}, \varepsilon_1) = \boldsymbol{0} \tag{22}$$

The relation in Eq. (21) links the low-thrust acceleration of Eq. (1) to the one that can be provided by a "pseudo solar-sail", given by Eq. (2) with $a_c = a_{\max}$ and no constraints on the thrust direction (or cone angle α). The solution of $\boldsymbol{\Phi}_1(\boldsymbol{z}, 1) = \boldsymbol{0}$, for which $\alpha \in [-\pi, \pi]$, is used as initial guess for the computation of the real-solar-sail OCP through a single-shooting approach. This consists in the computation of the zeros of $\boldsymbol{\Phi}_1(\boldsymbol{z}, 1) = \boldsymbol{0}$ subject to the constraint $\alpha \in \left[-\frac{\pi}{2}, \frac{\pi}{2} \right]$. In all the numerical test cases performed, the pseudo solar-sail solution always proved to be a good initial guess for the direct computation of the real solar-sail solution. A continuation strategy on the boundaries of the thrust cone angle [28] did not prove to be necessary.

If the desired characteristic acceleration is different with respect to the corresponding low-thrust acceleration (i.e. $a_c \neq a_{\max}$), a second homotopy and continuation is introduced on the characteristic acceleration, to link the initial solar-sail solution with $a_c = a_{c,0} = a_{\max}$ to the final one, which is characterized by $a_c = a_{c,f} \neq a_{\max}$:

$$\boldsymbol{f}_a = \left[(1-\varepsilon_2)a_{c,0} + \varepsilon_2 a_{c,f}\right]\left(\left(\frac{r_\oplus}{r}\right)^2 \cos^2\alpha\right)\begin{bmatrix}\cos\alpha \\ \sin\alpha\end{bmatrix} \tag{23}$$

in which $\varepsilon \equiv \varepsilon_2$. In this case, the corresponding homotopy is given by

$$\boldsymbol{\Phi}_2(\boldsymbol{z}, \varepsilon_2) = \mathbf{0} \tag{24}$$

As mentioned, the numerical continuation is used to continue and follow the solutions of the homotopy until eventually compute the desired solar-sail solution.

B. Transformed optimal control problem formulation

The PMP conditions stated in Sec. II.C assume a different form only when Eq. (21) is introduced in the equations of the dynamics; this does not occur when Eq. (23) is taken into account, because in this case a planar solar-sail OCP is solved and numerical continuation is only performed to decrease the characteristic acceleration. The main differences are in the formulation of the dynamics and in the optimal control law. Because a planar approximation is assumed in the homotopic transformation, the dynamics are now described as:

$$\dot{\boldsymbol{x}} = \begin{bmatrix} u \\ \dfrac{v}{r} \\ \dfrac{v^2}{r} - \dfrac{\mu}{r^2} + \boldsymbol{f}_{a,LTSS}\cdot\hat{\boldsymbol{r}} \\ -\dfrac{uv}{r} + \boldsymbol{f}_{a,LTSS}\cdot\hat{\boldsymbol{\vartheta}} \end{bmatrix} \tag{25}$$

The expression of the Hamiltonian function, depending only on the control variables $\bar{u}$ and α, is

$$\tilde{H} = \boldsymbol{\lambda}\cdot\boldsymbol{f}_{a,LTSS} = A\sin\alpha + B\cos\alpha + C\cos^3\alpha + D\sin\alpha\cos^2\alpha \tag{26}$$

in which

$$A = \lambda_v\left((1-\varepsilon)\bar{u}a_{\max}\right),\ B = \lambda_u\left((1-\varepsilon)\bar{u}a_{\max}\right),\ C = \lambda_u\left(\varepsilon a_{\max}\left(\frac{r_\oplus}{r}\right)^2\right),\ D = \lambda_v\left(\varepsilon a_{\max}\left(\frac{r_\oplus}{r}\right)^2\right) \tag{27}$$

The optimal control variables are the control angle α and the low-thrust non-dimensional control $\bar{u}$. The first order optimality condition for α implies that

$$\frac{\partial \tilde{H}}{\partial \alpha} = (A+D)\tau^6 + 2(B+3C)\tau^5 + (A-11D)\tau^4 + 4(B-3C)\tau^3 - (A-11D)\tau^2 + 2(B+3C)\tau - (A+D) = 0$$

(28)

in which $\tau = \tan\left(\frac{\alpha}{2}\right)$, thus $\alpha = 2\tan^{-1}(\tau)$. On the hypothesis that no singular arcs occur, the first-order optimality condition for $\bar{u}$ implies that

$$\bar{u} = \begin{cases} 1 & \text{if} \quad (\lambda_u \cos\alpha + \lambda_v \sin\alpha) < 0 \\ 0 & \text{if} \quad (\lambda_u \cos\alpha + \lambda_v \sin\alpha) > 0 \end{cases} \tag{29}$$

Note again that this hypothesis is numerically verified in all the numerical cases tested.

It should be noted that no analytical expressions exist for the roots of the sixth order polynomial of Eq. (28), for the generic case in which both $\lambda_u, \lambda_v \neq 0$. A closer analysis of Eq. (28) reveals that a full analytical solution is available only when $\lambda_u = 0,\ \lambda_v \neq 0$ or $\lambda_v = 0,\ \lambda_u \neq 0$. In addition, the polynomial roots of Eq. (28) are in the form of pairs $(\alpha, \pi + \alpha)$. However, these properties do not seem to give any contribution in understanding *a priori* the structure of the optimal cone angle. Considering also that the control variables $\bar{u}$ and α are nonlinearly dependent on each other, it turns out that the optimal control can be only found via an algorithm that can numerically compute the values of $\bar{u}$ and α that minimize $\tilde{H}$. In particular, the strategy adopted consists in the numerical computation of the real roots of the polynomial expression of Eq. (28) for $\bar{u} = \{0,1\}$ and then evaluating, for each set of solutions $(\alpha, \bar{u})$, the value of $\tilde{H}$. The optimal control is retrieved from the set of solutions $(\alpha, \bar{u})$ for which $\tilde{H}$ is minimum. The use of a numerical solver to find the polynomial roots of Eq. (28) could potentially result in an inaccurate computation of the derivative of the shooting function. However, the process of resolution of the shooting function proved to be always stable in all the numerical cases tested.

C. Transversality condition avoidance

The differential equations of the costates are homogenous, as it can be evinced, for instance, by their explicit formulation for the planar case:

$$
\begin{aligned}
\dot{\lambda}_r &= \lambda_u\left(\frac{v^2}{r^2}-\frac{2\mu}{r^3}+\frac{2\varepsilon a_c r_\oplus^2\cos^3\alpha}{r^3}\right)-\lambda_v\left(\frac{uv}{r^2}-\frac{2\varepsilon a_c r_\oplus^2\cos^2\alpha\sin\alpha}{r^3}\right)+\lambda_\vartheta\left(\frac{v}{r^2}\right)\\
\dot{\lambda}_\vartheta &= 0\\
\dot{\lambda}_u &= -\lambda_r+\lambda_v\left(\frac{v}{r}\right)\\
\dot{\lambda}_v &= -\lambda_\vartheta\left(\frac{1}{r}\right)+\lambda_v\left(\frac{u}{r}\right)-\lambda_u\left(\frac{2v}{r}\right)
\end{aligned}
\tag{30}
$$

For the sake of conciseness and without losing of generality, the formulation of the costate equations given by Eq. (30) is considered throughout this section. It is easy to verify that the same demonstration is also valid for the 3D case. Define $\bar{\boldsymbol{\lambda}}(t_0)$ the vector of the initial costates for which the transversality condition on the Hamiltonian is verified, as stated in Eq. (11). If an optimization algorithm is able to find initial values for the costates such that $\boldsymbol{\lambda}(t_0)=\bar{a}\bar{\boldsymbol{\lambda}}(t_0)$ with $\bar{a}\in\mathbb{R}^+$, this proportionality relation holds at any time $t\in\left[t_0,t_f\right]$, due to the homogeneity of Eq. (30). Furthermore, if such costates are considered, the first-order optimality conditions provided by Eq. (28) and Eq. (29) are unchanged. This implies that the optimal control laws and, thus, the entire dynamics of the rendezvous problem are also unaffected. However, the transversality condition on the Hamiltonian turns into

$$
H\left(t_f\right)-\boldsymbol{\lambda}\left(t_f\right)\cdot\frac{\partial\bar{\mathbf{x}}_f}{\partial t_f}=-\bar{a}
\tag{31}
$$

The transversality condition of Eq. (31) implies that the OCP cost function is $J=\bar{a}t_{0f}$, which is the same as considering Eq. (7). Therefore, the transversality condition on the Hamiltonian is negligible and can be excluded in the OCP formulation, if a minimum-time transfer problem is considered.

By adopting a constraint reduction, heuristic solvers can compute a solution for minimum-time transfer problems more easily. Indeed, equality constraints (such as the transversality condition on the Hamiltonian) can "narrow considerably the search space in which feasible solutions can be located" [14, 15]. For these reasons and for a matter of consistency, the transversality condition on the Hamiltonian has been excluded in all the numerical cases tested in this paper, both when heuristic and deterministic solvers have been used. To test the validity of the results, Eq. (31) was verified *a posteriori* on all the numerical test cases carried out and it was found that this relation was always verified for real positive values of $\bar{a}$. As result of neglecting the transversality condition on the Hamiltonian, $\boldsymbol{\Phi}(\boldsymbol{z},\varepsilon)=\mathbf{0}$

reduces to an underdetermined system of nonlinear equations: that is, a least-square numerical solver [35] is needed to find the solutions of such system. Nevertheless, it has been empirically verified that this approach is both numerically stable and faster than solving a square system, at least for the test cases considered.

D. Numerical continuation

The zeros of the solar-sail shooting function can be computed by using numerical continuation, starting from the low-thrust solution. In fact, this technique allows to follow the so-called "zero-path" of the homotopy (i.e. the locus of solutions $(\mathbf{z}, \varepsilon)$ of the system $\mathbf{\Phi}(\mathbf{z}, \varepsilon) = \mathbf{0}$) by continuing the parameter ε, starting from the solution at $\varepsilon = 0$ until computing the final solution at $\varepsilon = 1$. The numerical continuation algorithm adopted in the current work is implemented in the form of discrete continuation [22, 27]. It consists of progressively increasing the value of the parameter ε and, for each step, computing the solution of an intermediate OCP. Each intermediate solution is used as a starting point for the computation of the following problem until the final solution is computed. The continuation step size is adaptively determined: if convergence is achieved at an intermediate iteration, the algorithm doubles the step size to speed up the continuation process; if no convergence is achieved, the step size is halved and the continuation iteration is run again with a decreased step size until convergence is reached. If the step size is reduced down to its minimum preset value, the algorithm terminates without converging.

IV. Numerical test cases

This section presents four numerical test cases. Two test cases on solar sail Earth-Mars rendezvous are firstly considered to validate the homotopic approach. In these tests, the homotopic approach is compared with a classical solution method, based on the use of a heuristic solver. Two additional test cases on Earth-Apophis rendezvous assess the performances of the homotopic method in computing optimal solar-sail transfers to an object with a moderate orbital eccentricity. Keplerian elements of Mars and Apophis are in Table 1. The Earth orbit is considered circular with radius of 1 AU .

Table 1. Keplerian elements of the target objects on February, 14th 2016.

Object	a, AU	e	i, deg	Ω, deg	ω, deg	ν, deg
Mars	1.52	0.093	1.85	49.7	286.7	217.6
(99942) Apophis[1]	0.92	0.191	3.33	204.5	126.4	283.4

A. Validation of the homotopic approach: Earth-Mars rendezvous

Initially, the problem of coplanar circular-to-circular Earth-Mars rendezvous is considered. The minimum-time solar-sail rendezvous problem is solved by means of both the homotopy method and a conventional evolutionary method, within the same Hamiltonian formulation. Two test cases (named "test case 1" and "test case 2") are considered for the purpose of (a) validating the homotopic approach proposed and (b) comparing it with a method based on the use of a genetic algorithm (GA) for computing minimum-time solar-sail transfers. The test cases differ from each other on the sail's characteristic acceleration: $a_c = 1\ \mathrm{mm/s^2}$ in test case 1, whereas $a_c = 0.1\ \mathrm{mm/s^2}$ in test case 2. It should be mentioned that the homotopic approach was already tested in [36], on the simplest case of a circular-to-circular Earth-Mars orbit transfer with $a_c = 1\ \mathrm{mm/s^2}$. In that study, the solution computed by means of the homotopy method proves to be in perfect agreement with both the solution found by the genetic algorithm and the one shown in [37].

The low-thrust solution used to initialize the homotopy method is obtained via an indirect approach, for the orbit transfer case with $a_{\max} = 1\ \mathrm{mm/s^2}$. The planar transfers obtained by the homotopy method are used to compute the 3D rendezvous considering the real ephemerides of Mars, as shown in Table 1. This is done by means of a single shooting approach for both test case 1 and 2.

As previously mentioned, a genetic algorithm is also used in the first two test cases to solve the solar-sail OCPs. This is done only for the case of coplanar transfers between circular orbits, for a fair comparison between the GA and the homotopy method. The objective function to be minimized is the $\ell^2-\mathrm{norm}$ of the shooting function. Twenty

[1] Data available online at https://cneos.jpl.nasa.gov/orbits/elements.html [retrieved 08 August 2015].

different sets of settings have been considered for the GA simulations, differing in the population size ($Population = \{50,100,150,200,500\}$) and the maximum number of generations allowed ($MaxGenerations = \{500,1000,1500,2000\}$). Because of the heuristic nature of the GA, each set of settings has been run 100 times and statistical values have been taken into account for the comparison. Moreover, the solutions from GA have been refined by means of a gradient-based method, which is implemented in the "interior-point" algorithm in the MATLAB function *fmincon*.

The tolerances on the final position and velocity have been set to 1000 km for the position error and $0.1\ \mathrm{m/s}$ for the velocity errors, as stated in [37]. These tolerances are the same for all the test cases taken into account in this work. It is also worth mentioning that a C++ implementation of the Bulirsch-Stoer algorithm has been used to propagate the equations of the dynamics [38]. The absolute and relative tolerances for the propagator have both been set to 10^{-8} [37]. All the simulations have been performed in MATLAB on a 3.4 GHz Core i7-3770 with 16 GB of RAM, running Linux Ubuntu 14.04.

Test case 1. The launch date is fixed on February, 14th 2016. Table 2 shows the results of both the homotopy and the GA. The results for GA are expressed in terms of success rate of each set of settings, which is the percentage of runs (out of 100) that terminate with at least one feasible solution (a solution within the required tolerances). It is important to note that the success rates among all the sets of settings considered are below the 40%. The second column of Table 2 shows the number of sets with a success rate above 30% for the GA (because the homotopy method consists of a deterministic approach, it can be either successful or not successful). For the GA, the computational time is the lowest average computational time among all the sets of settings with a success rate above 30%. In Table 2, the minimum and maximum values of the time of flight are shown for the GA. Table 2 shows that the result obtained via the homotopy approach is consistent with the one obtained via the GA method, with a comparable computational time.

Table 2. Numerical results for coplanar circular-to-circular Earth-Mars rendezvous (a_c = 1 mm/s^2).

Method	Sets with success rate above 30%	Computational time, s	t_{0f} , days
Homotopy	-	27	429.58
GA	5 out of 20	27	429.57 (min), 429.59 (max)

Figure 2a shows the evolution of the cone angle over time during the first continuation (from low-thrust to pseudo solar-sail). The curve relative to the low-thrust solution is represented by a thick dashed line, whereas the curve for the pseudo solar-sail solution is in a thick continuous line. Figure 2b shows a comparison between the low-thrust and the solar sail cone angles over time. Note that the low-thrust cone angle over time is the same in both panels. Figure 3a and Fig 3b show the low-thrust and solar-sail transfer trajectories, respectively.

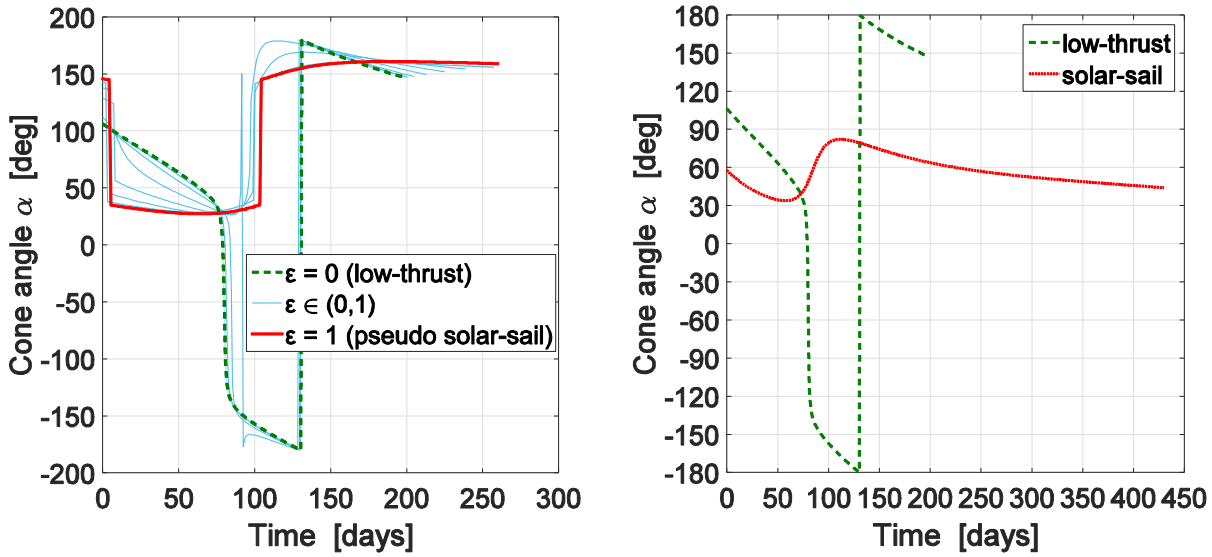

a) **b)**

Fig 2. Control history for coplanar circular-to-circular Earth-Mars rendezvous (a_c = 1 mm/s^2). (a) Cone angle evolution during the first continuation. (b) Low-thrust and solar sail cone angle.

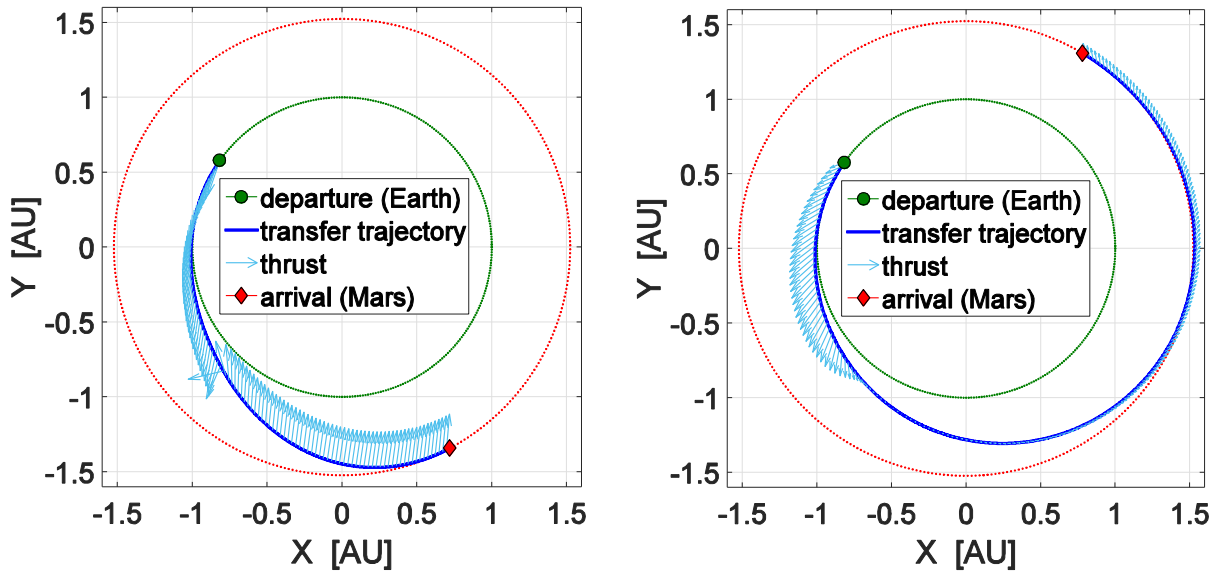

Fig 3. Transfer trajectories for coplanar circular-to-circular Earth-Mars rendezvous (a_c = 1 mm/s^2). (a) Low-thrust. (b) Solar-sail.

The 3D Earth-Mars solar-sail rendezvous is computed by means of a direct shooting approach, starting from the (2D) solution obtained by the homotopy method. The computational time spent in the direct shooting solution is of the order of fractions of second: the solution time of flight is $t_{0f} = 395.9$ days . Figure 4 shows both the X-Y and X-Z projections of the Earth-Mars rendezvous trajectory, whereas Fig 5 shows the cone and clock angles over time for the same rendezvous transfer.

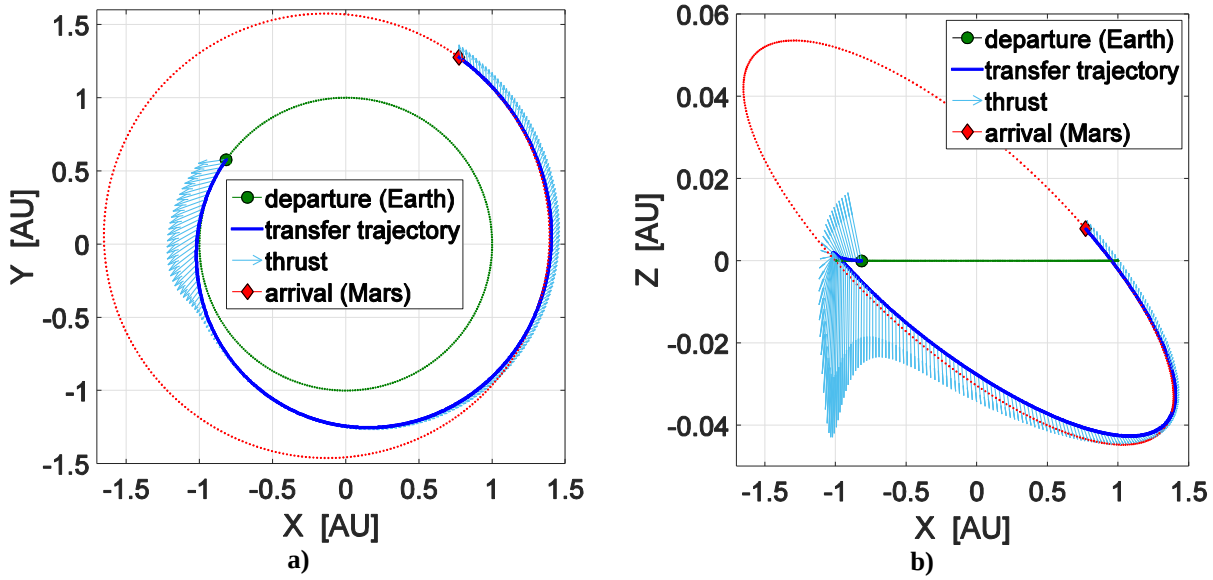

Fig 4. Transfer trajectory for the solar-sail Earth-Mars rendezvous (a_c = 1 mm/s^2). (a) X-Y plot. (b) X-Z plot. (Z-axis is not to scale).

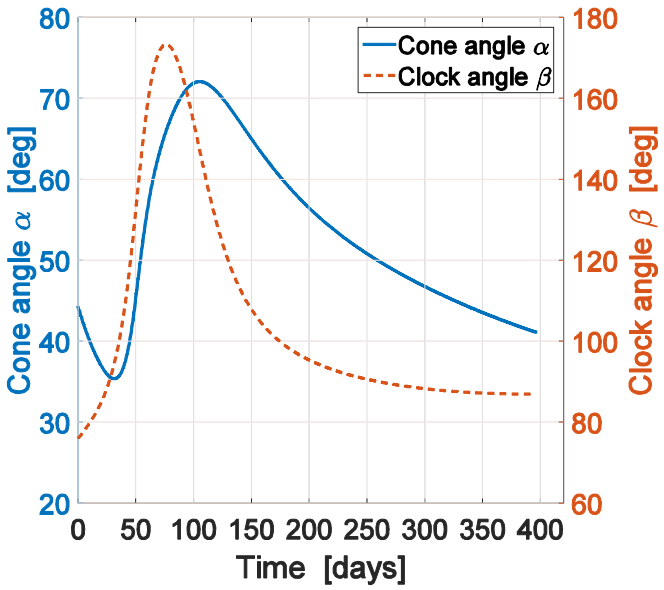

Fig 5. Control history for the solar-sail Earth-Mars rendezvous (a_c = 1 mm/s^2).

Note that the time of flight of the 3D solution is lower than that of the planar solution. While it might seem counterintuitive, there are two occurring reasons for this. The first is that the 3D transfer was computed using Mars' ephemerides, instead of a planar circular orbit. In addition, in a 3D transfer scenario, a solar sail can potentially thrust in a direction $\hat{\boldsymbol{n}}$ closer to the ideal direction $\hat{\boldsymbol{n}}^*$ given by the primer vector. This involves a reduction of the transfer duration that can also result in a time of flight of the 3D transfer shorter than the one of the planar transfer. This event occurs in the current test case. To show this, denote with Δn the integral average over time given by $\Delta n = \int_{t_0}^{t_f} \left\| \hat{\boldsymbol{n}}^* - \hat{\boldsymbol{n}} \right\| dt \Big/ t_{0f}$. The lower this value, the closer the solar-sail can thrust along $\hat{\boldsymbol{n}}^*$. In the current test case, it is numerically verified that the value of Δn in the 3D case is lower than in the planar case, that is $\Delta n_{3D} < \Delta n_{2D}$.

Test case 2. A continuation on the characteristic acceleration is performed, starting from the solution for the coplanar circular-to-circular Earth-Mars rendezvous of test case 1. In this way, the solar-sail rendezvous with $a_c = 0.1 \text{ mm/s}^2$ is computed by means of the homotopy method. Again, this same transfer is computed both by homotopy and genetic algorithm, for comparison purposes. The GA has been used with only one set of settings (*Population* = 500, *MaxGenerations* = 10000). The numerical results for both the homotopy and GA methods are shown in Table 3.

Table 3. Numerical results for coplanar circular-to-circular Earth-Mars rendezvous (a_c = 0.1 mm/s^2).

Method	Success rate (over 100 runs)	Computational time, s	t_{0f}, days
Homotopy	-	30	3291.20
GA	20%	1219	3773.23

Although the results, in terms of transfer trajectory and time of flight, have a purely academic interest, it is important to note the superior performances of the homotopy method with respect to the GA in terms of computational effort. In addition, it should be remarked the significant difference, in terms of transfer time, found by the two methods. Although the GA searches for a global solution, within a certain statistical confidence, cases occur in which a better solution exist but can be more difficult to be found by the heuristic solver, as Table 3 shows. In fact, different local solutions exist and the homotopy method can compute a better solution, if the numerical continuation follows a zero-path leading to a better local minimum [36].

As before, a single shooting approach has been used to compute the three-dimensional Earth-Mars rendezvous, starting from the solution obtained via the homotopy method and shown in Table 3. The computational time spent in the direct shooting solution is of the order of fractions of second, and the 3D transfer time of flight is $t_{0f} = 3287$ days.

Discussion. As a result of the numerical test cases on Earth-Mars rendezvous, the homotopy method shows good performances in the computation of minimum-time solar-sail trajectories. This is particularly evident when lower values of the sail's characteristic acceleration are considered.

Lastly, it is important to mention that the proposed homotopy method requires initialization with a solution, consisting of a low-thrust transfer reasonably close to a minimum-time low-thrust rendezvous. In fact, the low-thrust solution used in test case 1 (consisting of a coplanar circular-to-circular orbit transfer) is close to a rendezvous transfer performed at the same launch epoch chosen for this test case. If a different launch date needs to be considered, the planar solar-sail transfer computed for test case 1 can be used to initialize a continuation process performed on the initial relative longitude between Earth and Mars [36]. The continuation terminates when such angle equals to the initial relative longitude corresponding to the desired launch date.

B. Transfers to object with moderate eccentricity: Earth-Apophis rendezvous

The numerical cases tested in this section aim to validate the proposed homotopy method for more complex scenarios, involving transfers to objects with moderate eccentricity. The mission scenario consists in a rendezvous transfer from Earth to asteroid (99942) Apophis. The results shown in [39] are used as a mean of comparison and validation.

The departure from the Earth takes place on July, 28th 2017, as in [39]. Two test cases have been considered (named "test case 3" and "test case 4"), differing only by the value of the sail's characteristic acceleration. In test case 3, $a_c = 0.6 \text{ mm/s}^2$, corresponding to a sail lightness number $\gamma = 0.02$, whereas, in test case 4, $a_c = 0.12 \text{ mm/s}^2$, corresponding to $\gamma = 0.1$ [34]. The two values correspond to the extreme values in the range of the sail lightness numbers considered in [39], for a solar-sail-only transfer. The solar-sail rendezvous of test case 3 is initially computed in the planar case, by means of the first homotopic continuation. The homotopy method is initialized by a solution (computed via the indirect approach) consisting into a planar minimum-time low-thrust rendezvous with $a_c = 0.6 \text{ mm/s}^2$. The planar rendezvous solution of test case 3 is used in turn to initialize the second homotopic continuation, for computing the planar rendezvous transfer for test case 4. Finally, the planar rendezvous solutions are used to compute the three-dimensional solar-sail rendezvous, for both test case 3 and 4, with a direct shooting. The results of the two numerical cases presented in this section are summarized in Table 4 and compared with the findings in [39].

Table 4. Optimal solar-sail rendezvous from Earth to (99942) Apophis

Test case	a_c, mm/s^2	t_{0f}, days	Computational time, s
Test case 3 (planar transfer)	0.6	457	28
Test case 3 (3D transfer)		459	28
Test case 3 (Ref. [39])		468	-
Test case 4 (planar transfer)	0.12	1160	29
Test case 4 (3D transfer)		1230	29
Test case 4 (Ref. [39])		1260	-

Again, the single shooting approach used to compute the 3D solutions requires only fractions of a second to converge. Therefore, the computational time required to compute the 3D solutions is neglected in Table 4. As shown in the table, the results of the Earth-Apophis rendezvous of test case 3 and 4 are in good agreement with the results presented in [39]. Figure 6 and Fig 7 show the minimum-time solar-sail trajectories and the cone and clock angle over time, for $a_c = 0.6$ mm/s^2 and $a_c = 0.12$ mm/s^2, respectively.

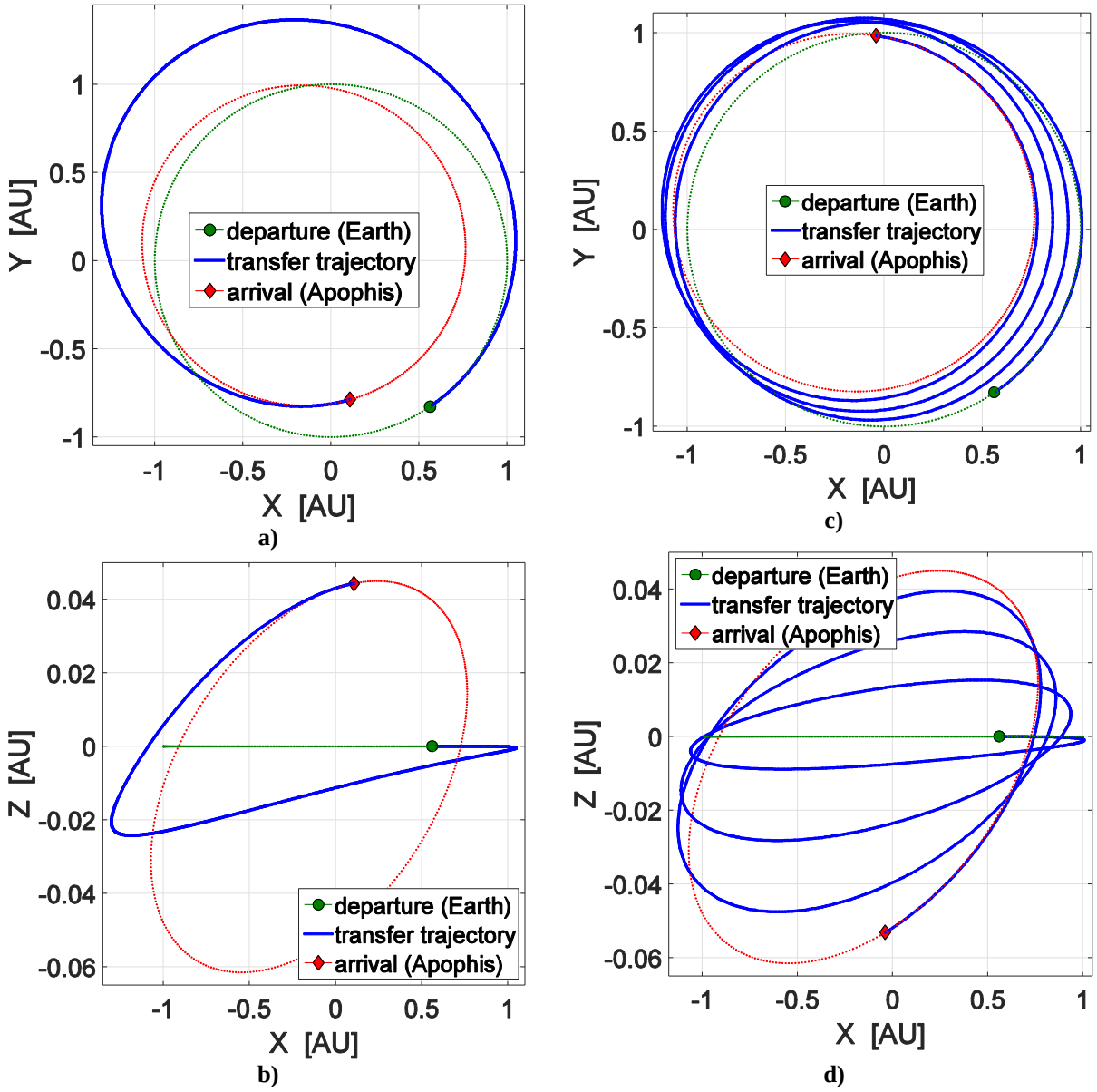

Fig 6. 3D transfer trajectory for the Earth-Apophis solar-sail rendezvous. (a) X-Y and (b) X-Z plot with a_c = 0.6 mm/s^2. (c) X-Y and (d) X-Z plot with a_c = 0.12 mm/s^2. (Z-axis is not to scale).

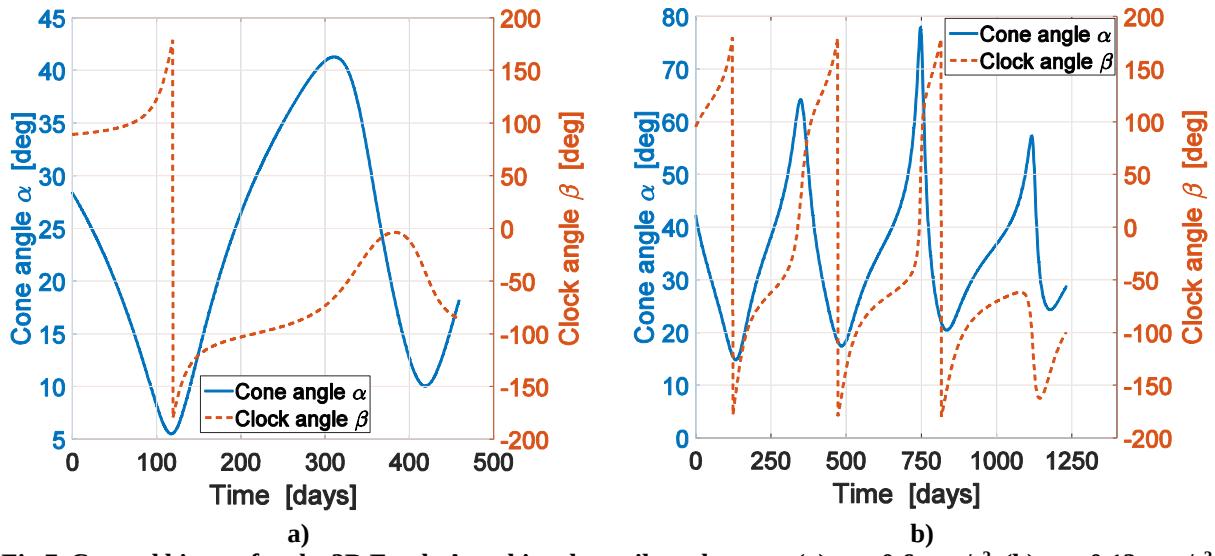

Fig 7. Control history for the 3D Earth-Apophis solar-sail rendezvous. (a) a_c = 0.6 mm/s^2. (b) a_c = 0.12 mm/s^2.

The proposed homotopic approach allows to compute optimal solar-sail trajectories for a wide range of characteristic accelerations, in a single and fast run. This is achieved by means of the continuation on the characteristic acceleration, in which intermediate solutions with $a_c \in \left[a_{c,0}, a_{c,f}\right]$ are computed at each successful iteration. Other approaches would usually require a single optimization to be performed for each value of the characteristic acceleration, leading to a higher computational effort to obtain the entire family of solutions, making this method particularly appealing for preliminary mission design. In fact, the early stages of a solar-sail mission planning are usually characterized by an uncertainty on the value of the sail characteristic acceleration. For instance, Ref. [40] shows the value of the characteristic acceleration as function of the sail size for the DLR/ESA Gossamer Roadmap to solar sailing. A preliminary mission is described in [40] which considers a characteristic acceleration $a_c = 0.3$ mm/s^2 and a sail size in the range between $(54\ \text{m})^2$ and $(65\ \text{m})^2$, depending on the bus mass taken into account. One of the improvements outlined in [40] is to find a solar-sail trajectory, within the same mission criteria, with a lower value of the characteristic acceleration. As an example, Fig 8 shows a plot for the minimum time of flight t_{0f} as function of a_c (computed by means of the second homotopic continuation) in the case of the Earth-Apophis planar rendezvous with characteristic acceleration bounded in $a_c \in [0.12, 0.6]$ mm/s^2. A time of flight of about 660 days is needed if a sail with a characteristic acceleration $a_c = 0.3$ mm/s^2 is considered.

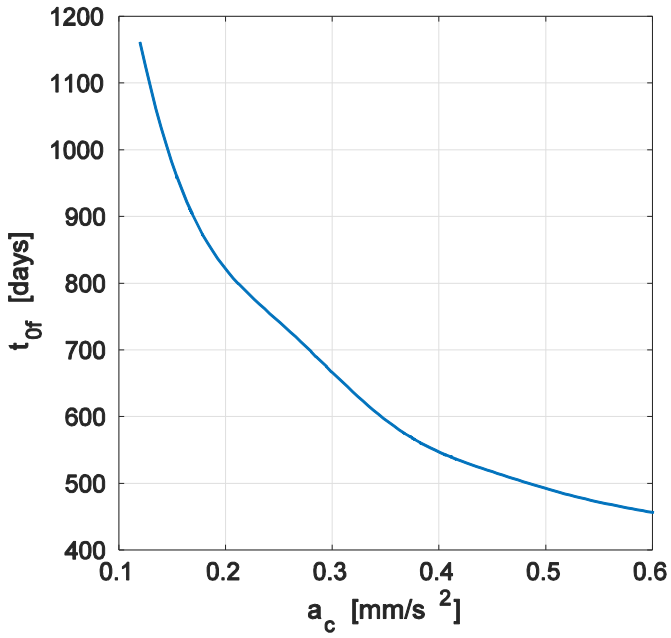

Fig 8. Minimum time of flight as function of the characteristic acceleration for the coplanar Earth-Apophis case.

V. Conclusions

In this paper, the homotopic approach is used to compute minimum-time solar-sail rendezvous transfers starting from a low-thrust solution for a similar problem, computed in the planar approximation. The low-thrust solution is assumed given as it is normally easy to find numerically. By adopting the homotopic approach, the low-thrust solutions are converted into 2D optimal solar-sail trajectories. These solutions are used to compute 3D solar sail trajectories, using a single shooting, assuming small inclination change. Numerical test cases are shown for Earth-Mars and Earth-Apophis rendezvous transfers. Both the homotopic approach and the genetic algorithm are used to compute minimum-time solar-sail transfers, for the case of planar circular-to-circular Earth-Mars rendezvous and within the same formulation of the optimal control problem. The advantage of the proposed technique is in obtaining precise solutions for solar-sail minimum-time problems with a little computational effort, with respect to a conventional solver, such as a genetic algorithm. These advantages are particularly evident when low characteristic accelerations are considered. The numerical efficiency of the proposed method is also proved for the computation of solar-sail trajectories to an

object with a moderate orbital eccentricity, as shown in the transfer to Apophis. The homotopic approach is particularly suitable as a preliminary mission design tool, to quickly compute minimum-time solar-sail trajectories within a wide range of characteristic accelerations.

Acknowledgments

Alessandro Peloni gratefully acknowledges support for this research from the School of Engineering at the University of Glasgow and the Engineering and Physical Sciences Research Council for funding part of this research under the James Watt sponsorship program, award number 1370838.

References

[1] Betts, J. T., *Practical Methods for Optimal Control and Estimation Using Nonlinear Programming (Second Edition)*, Soc. for Industrial and Applied Mathematics, Philadelphia, PA, 2010, pp. 91,123-126.

[2] Hull, D. G., *Optimal Control Theory for Applications*, Mechanical Engineering Series, Springer, New York, NY, 2003, pp. 11,12,293.

[3] Conway, B. A., *Spacecraft Trajectory Optimization*, Cambridge University Press, 2010, pp. 1-7,16-36.

[4] Sauer, C. G. J., "Optimum Solar-Sail Interplanetary Trajectories", *AIAA/AAS Astrodynamics Conference*, AIAA Paper 76-792, 1976.

[5] Colasurdo, G. and Casalino, L., "Optimal Control Law for Interplanetary Trajectories with Nonideal Solar Sail", *Journal of Spacecraft and Rockets*, Vol. 40, No. 2, 2003, pp. 260-265.

doi: 10.2514/2.3941

[6] Mengali, G. and Quarta, A. A., "Optimal Three-Dimensional Interplanetary Rendezvous Using Non-Ideal Solar Sail", *Journal of Guidance, Control, and Dynamics*, Vol. 28, No. 1, 2005, pp. 173-177.

doi: 10.2514/1.8325

[7] Mengali, G. and Quarta, A. A., "Rapid Solar Sail Rendezvous Missions to Asteroid 99942 Apophis", *Journal of Spacecraft and Rockets*, Vol. 46, No. 1, 2009, pp. 134-140.

doi: 10.2514/1.37141

[8] Zeng, X., Gong, S. and Li, J., "Fast solar sail rendezvous mission to near Earth asteroids", *Acta Astronautica*, Vol. 105, No. 1, 2014, pp. 40-56.

doi: 10.1016/j.actaastro.2014.08.023

[9] Heiligers, J., Ceriotti, M., McInnes, C. R. and Biggs, J. D., "Displaced Geostationary Orbit Design Using Hybrid Sail Propulsion", *Journal of Guidance, Control, and Dynamics*, Vol. 34, No. 6, 2011, pp. 1852-1866.

doi: 10.2514/1.53807

[10] Peloni, A., Ceriotti, M. and Dachwald, B., "Solar-Sail Trajectory Design for a Multiple Near-Earth-Asteroid Rendezvous Mission", *Journal of Guidance, Control, and Dynamics*, Vol. 39, No. 12, 2016, pp. 2712-2724.

doi: 10.2514/1.G000470

[11] Wawrzyniak, G. G. and Howell, K. C., "Numerical techniques for generating and refining solar sail trajectories", *Advances in Space Research*, Vol. 48, No. 11, 2011, pp. 1848-1857.

doi: 10.1016/j.asr.2011.04.012

[12] Sood, R. and Howell, K. C., "L4, L5 Solar Sail Transfers and Trajectory Design: Solar Observations and Potential Earth Trojan Exploration", *26th AAS/AIAA Space Flight Mechanics Meeting*, AAS Paper 16-467, 2016.

[13] Dachwald, B., "Optimization of very-low-thrust trajectories using evolutionary neurocontrol", *Acta Astronautica*, Vol. 57, 2005, pp. 175-185.

doi: 10.1016/j.actaastro.2005.03.004

[14] Pontani, M. and Conway, B. A., "Optimal Low-Thrust Orbital Maneuvers via Indirect Swarming Method", *Journal of Optimal Theory and Applications*, Vol. 162, No. 1, 2014, pp. 272-292.

doi: 10.1007/s10957-013-0471-9

[15] Pontani, M. and Conway, B. A., "Particle Swarm Optimization Applied to Space Trajectories", *Journal of Guidance, Control, and Dynamics*, Vol. 33, No. 5, 2010, pp. 1429-1441.

doi: 10.2514/1.48475

[16] Mengali, G. and Quarta, A. A., "Tradeoff Performance of Hybrid Low-Thrust Propulsion System", *Journal of Spacecraft and Rockets*, Vol. 44, No. 6, 2007, pp. 1263-1270.

doi: 10.2514/1.30298

[17] Rao, A. V., "Survey of Numerical Methods for Optimal Control", *2009 AAS/AIAA Astrodynamics Specialist Conference*, AAS Paper 09-334, 2009.

[18] Whitehead, G. W., *Elements of Homotopy Theory*, Graduate Texts in Mathematics, Springer, New York, NY, 1978, pp. 3-8.

[19] Allgower, E. L. and Georg, K., "Numerical path following," *Handbook of Numerical Analysis*, edited by P.G. Ciarlet and J.L. Lions, 1997, pp. 5-7.

[20] Allgower, E. L. and Georg, K., *Introduction to Numerical Continuation Methods*, Soc. for Industrial and Applied Mathematics, Philadelphia, PA, 2003, pp. 1-6.

[21] Bertrand, R. and Epenoy, R., "New smoothing techniques for solving bang–bang optimal control problems—numerical results and statistical interpretation", *Optimal Control Applications and Methods*, Vol. 23, No. 4, 2002, pp. 171-197.

doi: 10.1002/oca.709

[22] Haberkorn, T., Martinon, P. and Gergaud, J., "Low Thrust Minimum-Fuel Orbital Transfer: A Homotopic Approach", *Journal of Guidance, Control, and Dynamics*, Vol. 27, No. 6, 2004, pp. 1046-1060.

doi: 10.2514/1.4022

[23] Li, J. and Xi, X.-N., "Fuel-Optimal Low-Thrust Reconfiguration of Formation- Flying Satellites via Homotopic Approach", *Journal of Guidance, Control, and Dynamics*, Vol. 35, No. 6, 2012, pp. 1709-1717.

doi: 10.2514/1.57354

[24] Caillau, J. B., Gergaud, J. and Noailles, J., "3D Geosynchronous Transfer of a Satellite: Continuation on the Thrust", *Journal of Optimization Theory and Applications*, Vol. 118, No. 3, 2003, pp. 541-565.

doi: 10.1023/B:JOTA.0000004870.74778.ae

[25] Picot, G., "Shooting and numerical continuation methods for computing time-minimal and energy-minimal trajectories in the Earth-Moon system using low propulsion", *Discrete and Continuous Dynamical Systems - Series B*, Vol. 17, No. 1, 2012, pp. 245-269.

doi: 10.3934/dcdsb.2012.17.245

[26] Guo, T., Jiang, F. and Li, J., "Homotopic approach and pseudospectral method applied jointly to low thrust trajectory optimization", *Acta Astronautica*, Vol. 71, 2012, pp. 38-50.

doi: 10.1016/j.actaastro.2011.08.008

[27] Jiang, F., Baoyin, H. and Li, J., "Practical Techniques for Low-Thrust Trajectory Optimization with Homotopic Approach", *Journal of Guidance, Control, and Dynamics*, Vol. 35, No. 1, 2012, pp. 245-258.

doi: 10.2514/1.52476

[28] Geffroy, S. and Epenoy, R., "Optimal low-thrust transfers with constraints---generalization of averaging techniques", *Acta Astronautica*, Vol. 41, No. 3, 1997, pp. 133-149.

doi: 10.1016/S0094-5765(97)00208-7

[29] Tarzi, Z., Speyer, J. and Wirz, R., "Fuel optimum low-thrust elliptic transfer using numerical averaging", *Acta Astronautica*, Vol. 86, 2013, pp. 95-118.

doi: 10.1016/j.actaastro.2013.01.003

[30] Pan, B., Lu, P., Pan, X. and Ma, Y., "Double-Homotopy Method for Solving Optimal Control Problems", *Journal of Guidance, Control, and Dynamics*, Vol. 39, No. 8, 2016, pp. 1706-1720.

doi: 10.2514/1.G001553

[31] Dachwald, B. and Seboldt, W., "Multiple near-Earth asteroid rendezvous and sample return using first generation solar sailcraft", *Acta Astronautica*, Vol. 57, No. 11, 2005, pp. 864-875.

doi: 10.1016/j.actaastro.2005.04.012

[32] Wie, B., "Thrust Vector Control Analysis and Design for Solar-Sail Spacecraft", *Journal of Spacecraft and Rockets*, Vol. 44, No. 3, 2007, pp. 545-557.

doi: 10.2514/1.23084

[33] Mesterton-Gibbons, M., *A Primer on the Calculus of Variations and Optimal Control Theory*, American Mathematical Society, Providence, Rhode Island, 2009, pp. 141-146,177.

[34] McInnes, C. R., *Solar Sailing: Technology, Dynamics and Mission Applications*, Springer Praxis Publishing, Chichester, U.K., 1999, pp. 38-40,115-116.

[35] Moré, J. J., "The Levenberg-Marquardt algorithm: Implementation and theory", *Lecture Notes in Mathematics*, Vol. 630, 1978, pp. 105-116.

doi: 10.1007/BFb0067700

[36] Sullo, N., Peloni, A. and Ceriotti, M., "From Low Thrust to Solar Sailing: A Homotopic Approach", *26th AAS/AIAA Space Flight Mechanics Meeting*, AAS Paper 16-426, 2016.

[37] Mengali, G. and Quarta, A. A., "Solar sail trajectories with piecewise-constant steering laws", *Aerospace Science and Technology*, Vol. 13, No. 8, 2009, pp. 431-441.

doi: 10.1016/j.ast.2009.06.007

[38] Stoer, J. and Bulirsch, R., *Introduction to Numerical Analysis*, Springer, New York, NY, 2002, pp. 521-524.

[39] Gong, S., Li, J. and Jiang, F., "Interplanetary trajectory design for a hybrid propulsion system", *Aerospace Science and Technology*, Vol. 45, 2015, pp. 104-113.

doi: 10.1016/j.ast.2015.04.020

[40] Dachwald, B., Boehnhardt, H., Broj, U., Geppert, U. R. M. E., Grundmann, J.-T., Seboldt, W., et al., "Gossamer Roadmap Technology Reference Study for a Multiple NEO Rendezvous Mission," *Advances in Solar Sailing*, edited by M. Macdonald, Springer Praxis Books, Springer-Verlag, Berlin, 2014, pp. 211-226.